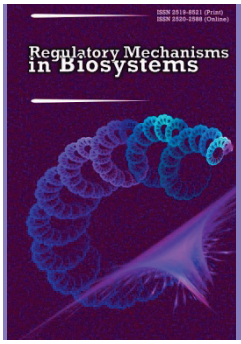

Regulatory Mechanisms in Biosystems

ISSN 2519-8521 (Print)
ISSN 2520-2588 (Online)
Regul. Mech. Biosyst.,
2023, 14(4), 552–558
doi: 10.15421/022380

The determination of fibroblast and keratinocyte death types after their transplantation into γ-irradiated porous scaffold *in vitro*

Y. H. Kot, K. V. Kot, R. A. Kurbanov

V. N. Karazin Kharkiv National University, Kharkiv, Ukraine

Article info

Received 01.09.2023
Received in revised form 05.10.2023
Accepted 18.10.2023

V. N. Karazin Kharkiv National University, Svobody sq., 4, Kharkiv, 61022, Ukraine.
Tel.: +38-093-973-17-73.
E-mail: yurii.kot@karazin.ua

Kot, Y. H., Kot, K. V., & Kurbanov, R. A. (2023). The determination of fibroblast and keratinocyte death types after their transplantation into γ-irradiated porous scaffold in vitro. Regulatory Mechanisms in Biosystems, 14(4), 552–558. doi:10.15421/022380

In the course of radiation therapy, normal cells surrounding the tumor are also irradiated. During and after irradiation, they undergo a series of structural and metabolic changes, which can lead to cell death or transformation. Therefore, when planning and conducting radiation therapy, the effects of radiation on normal cells are taken into account with the aim of predicting and further correcting post-radiation complications, including the development of radiation burns and ulcers. Radiation skin burns are characterized by a prolonged course of the wound healing process, which is accompanied by a sharp decrease in the number of viable cells in the affected tissue from the first hours of irradiation. The type of cell death can significantly impact the effectiveness of radiation therapy and post-radiation complication correction. Therefore, it is important to study the type of their death in irradiated three-dimensional culture on a model of irradiated dermal equivalent, which is widely used today for modeling biological processes. To detect the pathways of cell death, the levels of reactive oxygen species, cell viability, number of cells undergoing autophagy, apoptosis, and necrosis, the content of active caspases 3, 8, and 9 was fluorometrically measured in the irradiated 3D cell culture by laser scanning confocal microscopy. It was determined that the transplantation of fibroblasts and keratinocytes into the irradiated dermal equivalent contributed to an increase in the overall viability of cells of the equivalent and led to a significant decrease in the concentration of free oxygen forms in the irradiated equivalent. Cells within the irradiated equivalent were not evenly distributed in terms of their quantity and viability, with an overall decrease in the cell count over time. A cluster of equivalent cells with significantly higher viability was formed around the transplant. At the same time, the fibroblasts of the transplant were found to be more resistant to the cytotoxic factors of the post-irradiation culture environment compared to keratinocytes. It was demonstrated that non-irradiated dermal equivalent cells predominantly undergo cell death through autophagy, irradiated equivalent cells primarily undergo necrosis, and after the introduction of the transplant, cell death predominantly occurs through apoptosis. In irradiated culture, both with and without transplantation, there is an increase in the content of effector caspase 3. Cells in irradiated culture undergo apoptosis through the mitochondrial mechanism (with a predominance of active caspase 9), while in irradiated culture with the introduction of the transplant, the receptor-mediated mechanism of apoptosis dominates (with a predominance of active caspase 8). The obtained results can be important for the development of new effective methods of therapy for radiation burns, chronic ulcers and wounds of various etiologies.

Keywords: cell death; apoptosis; autophagy; necrosis; transplantation; γ-irradiation; reactive oxygen species; caspases.

Introduction

Previously, in an *in vivo* experiment, we demonstrated that the transplantation of autologous fibroblasts and keratinocytes into irradiated skin leads to the inhibition of radiation-induced skin ulcers and the restoration of the structure of the affected skin (Kot et al., 2015). This occurs due to the restoration of a pool of living actively synthesizing cells that have a system of positive feedback, stimulating mutual proliferation and synthetic activity. However, at the same time, it was shown that the regenerated skin has certain histological features and biochemical defects – a thicker and harder epidermal layer is formed, tissue sclerosing occurs, the content of pro-oxidant and pro-inflammatory markers in the radiation zone remains quite high. This may be a consequence of the predominance of unregulated forms of cell death in irradiated culture.

The current cell death classification system was last significantly updated in 2018 by the Nomenclature Committee on Cell Death (NCCD), which formulates principles for defining and interpreting all aspects of cell death (Hu et al., 2021). Currently, cell death can be fundamentally divided into regulated cell death (RCD) and accidental cell death (ACD). ACD can be triggered outside of possible control mechanisms. In contrast, RCD involves precise signaling cascades, is executed by a set of defined effector molecules, and has unique biochemical, functional, and immunological consequences (Galluzzi & Myint, 2023). RCD encompasses three major types of cell death. Type I cell death (apoptosis) is characterized by the decrease in cell volume, the loss of plasma membrane asymmetry, the formation of apoptotic bodies, the condensation and fragmentation of chromatin (Takács-Vellai, 2023). Type II cell death (autophagy) is characterized by specific vacuolization and promotion of survival of surrounding cells in most cases. However, in some cases, autophagy can induce autophagy-dependent death of microenvironment cells (Lu et al., 2022). Type III cell death (necrosis) is characterized by intense loss of plasma membrane integrity, accompanied by the saturation of the microenvironment with cell decay products (Zhang et al., 2022; Park et al., 2023).

An inevitable consequence of cell irradiation is the generation of reactive oxygen species (ROS), which are considered as specific cellular messengers capable of both promoting cell survival and adaptation, and inducing a certain type of cell death (Owusu et al., 2021; Villalpando-Rodriguez & Gibson, 2021). ROS-induced cell death occurs in both the transplant and the microenvironment of the transplant and is considered one of the key problems in transplantation and cell therapy (Van Erp et al., 2017; Machado et al., 2023). Biomolecules related to cell death are now being investigated as potential biomarkers for assessing the viability of donor

organs and their role in disease development (Shen et al., 2023; Zhao et al., 2023). Inhibitors for various types of cell death have been explored as potential therapeutics for managing injuries related to ischemia/reperfusion syndrome in organ transplantation or cell therapy following radiation therapy (Sia et al., 2020; Capuzzimati et al., 2022). The type of cell death induced by radiation depends on several factors, including cell type, radiation dose and quality (Jiao et al., 2022), oxygen tension (Rasouli et al., 2023), TP53 status (Brahme, 2023), DNA repair capacity, cell cycle phase at the time of radiation exposure (Obata et al., 2023), and the microenvironment (Arnold et al., 2018; Monjazeb et al., 2020).

Yoo et al. (2023) described that apoptosis was confirmed to occur later than autophagy in radiation treatment, and the inhibition of autophagy led to a decrease in apoptosis. Radiation-induced autophagy may be regulated by modulators such as IL6, IL1, TNFα, IL18, microRNAs like microRNA-7 and microRNA-7-5P, and ROS. Augmentation of autophagy results in increased cervical cancer cell death under radiation (Roy et al., 2022; Wu et al., 2023). Autophagy occurs to maintain stability and promote cell survival against radiation, thus contributing to cells' radioresistance (Lomonaco et al., 2009; Saleh et al., 2022). However, when autophagic activity becomes excessive and degradation overwhelms the cell's capacity, autophagy can lead to the death of irradiated cells and cells in the microenvironment (Zein et al., 2021).

Fibroblast and keratinocyte cell therapies have shown promising therapeutic effects in restoring damaged skin and promoting the functional repair of tissue in radiation-induced dermatitis. However, accumulating evidence has demonstrated the presence of increased concentrations of proinflammatory cytokines in cell-treated skin post-transplantation, which compromises the therapeutic efficiency of fibroblasts and keratinocytes.

Determination of cell death types and gaining a deeper understanding of the molecular mechanisms of cell death may help to improve preservation of donor cells and treatment of primary graft dysfunction during and after cell therapy.

The aim of the work was to investigate experimentally *in vitro* on a dermal equivalent model which type of cell death predominates when introducing a cell transplant into irradiated three-dimensional culture.

Materials and methods

Primary cells source and culturing. The experiments were performed with cryopreserved primary normal human dermal fibroblasts (PromoCell, C-12302) and normal human epidermal keratinocytes (PromoCell, C-12003). In the laboratory, cells were stored in Biorack 3000 cryogenic storage (Statebourne Cryogenics, UK). Immediately before culturing, cells were thawed and washed from cryoprotectant according to the standard protocol and their number, viability and size distribution were determined. Determination of the number, viability and size heterogeneity of cells in the primary cell suspensions was carried out by the method of measuring impedance in the flow, using an automatic cell counter Scepter 2.0 (Millipore, USA) and Scepter Software Pro 2.1. The primary cell suspensions were examined for the total number of cells ($1.5–1.7\times10^6$/mL), cell viability (92.0–94.0%) and the degree of heterogeneity in size (11–13 μm). Fibroblasts and keratinocytes were seeded at a density of 1.5×10^4 cells/well in a Millicell EZ SLIDE 8 (Merck Millipore, USA) well glass slide and allowed to grow in Dulbecco's Modified Eagle Medium (Gibco™, USA) supplemented with 10.0% Fetal Bovine Serum (Gibco™, USA), 2 mM L-glutamine (Invitrogen, USA) and 1.0% "Antibiotic-Antimycotic Solution" (Gibco™, USA) using a Galaxy 14S (Eppendorf, Germany) CO_2-incubator (37.0 ± 0.1 °C, 5.0 ± 0.1% CO_2, 99.5 ± 0.1% RH) for 10 days until 80.3% to 85.1% confluence. The non-adherent cells were removed after 48 h incubation after the first medium change. Fibroblast and keratinocyte cultures were tested for mycoplasma contamination using the "MycoAlert® Mycoplasma Detection Kit" (Lonza Inc., Switzerland) and a Sirius L luminometer (Titertek Berthold, USA).

Porous scaffold-based 3D cell culture formation. Cultivation of fibroblasts and keratinocytes in an immobilized state was carried out using the GEM – Global Eukaryotic Microcarrier technology, according to which cells are immobilized on the surface of spherical porous alginate microcarriers. Alginate microcarriers were prepared using the GEM Microcarrier Packs kit (Global Cell Solutions, cat. no. GEM-4133) and following the manufacturer's instructions. Because fibroblasts and keratinocytes have a high degree of adhesion to collagen and fibronectin, the alginate solution contained 1.0% collagen type 1 (Merck, cat. no. CC050) and 1.0% fibronectin (Merck, cat. no FC010). Microcarriers were stored at 4.0 °C in PBS until use. Before immobilization of cells, alginate microcarriers were washed three times with Dulbecco's Modified Eagle Medium (Gibco™, USA) and preheated to 37.0 °C. Cells were added to the suspension of alginate carriers at the rate of 0.5×10^6 each type of cells/ml of suspension. After 24 hours, the cells adhered to the surface of the microcarriers. Non-attached cells were removed when the nutrient medium was replaced. 15 mL of the microcarrier suspension with immobilized cells was placed in a LeviTube vial (OMNI Life Sciences, cat. no. #2800005) and cultured for 168 hours (37.0 ± 0.1 °C, 5.0 ± 0.1% CO_2, 99.5 ± 0.1% RH, mixing 5 revolutions/hour) in the CERO BioLevitator bioreactor (Omni Life Science GmbH & Co). The conditions for the production of media, immobilization and cultivation of fibroblasts and keratinocytes were in accordance with the current practice of dynamic cultivation of this type of cells (Hofmann et al., 2023; Tahri et al., 2023).

3D cell culture irradiation. Porous scaffold-based 3D cell culture was irradiated with the ROCUS AM (Co60) gamma complex. The irradiation dose was 0.75 Gy (104 kV, 9 mA; 0.2 Gy/minute; irradiation duration 225 seconds) and corresponded to the range of single doses used in radiation therapy. A single focal dose in clinical external beam radiation therapy is 0.3–5.0 Gy, while a single dose of 0.7–1.1 Gy is recommended as a tolerable single dose, which reduces the likelihood of radiation complications (Mott & West, 2021; Wong et al., 2021). An increase in the number of non-viable cells becomes probable at the 6th hour of observation. Since the effectiveness of the negative consequences of radiation damage correction is correlated with the time after irradiation, it is of greatest interest to evaluate the ability of normal fibroblasts and keratinocytes to correct the prooxidant status of cells in the first hours after irradiation, when irradiation has not yet led to significant cell death. Under the conditions of this experiment, the research time of 2 hours meets these requirements.

Cells transplantation into irradiated 3D cell culture. Two hours after irradiation, normal fibroblasts and keratinocytes were injected into irradiated porous scaffolds using micromanipulators TransferMan NK (Eppendorf) and CellTram Air pneumatic microinjector (Eppendorf) as part of IMT2 inverted microscope complex (Olympus). Cells were added directly to the center of each scaffold at the rate of 0.5×10^3 for each type of cells/scaffold. Normal cells-treated porous microcarriers were cultured for 8 days (37.0 ± 0.1 °C, 5.0 ± 0.1% CO_2, 99.5 ± 0.1% RH, mixing 5 revolutions/hour) in the CERO BioLevitator bioreactor (Omni Life Science GmbH & Co). Determination of the parameters reactive oxygen species content, cell viability, cell death types and active caspases content was performed after 2, 4 and 6 days of incubation.

Tracking of irradiated and transplanted cells. Two hours before irradiation, alginate scaffold-based 3D cell culture was incubated with vital blue fluorescence cell dye ($\lambda_{Ex}/\lambda_{Em}$ = 360/445 nm) as part of "CytoPainter Cell Tracking Staining Kit – Blue Fluorescence" (Abcam, ab187963). Two hours before transplantation, fibroblasts and keratinocytes were incubated with vital green and red fluorescence cell dyes ($\lambda_{Ex}/\lambda_{Em}$ = 490/520, $\lambda_{Ex}/\lambda_{Em}$ = 540/560 nm) as parts of "CytoPainter Cell Tracking Staining Kit – Green Fluorescence" (Abcam, ab187964) and "CytoPainter Cell Tracking Staining Kit – Red Fluorescence" (Abcam, ab187965) respectively. Determination of live cells' localization and migration into microcarriers was performed in 35 mm confocal dishes in Z-stack real-time mode by confocal microscopy FV10i-LIV (Olympus) equipped for prolonged cell viability in time-lapse experiments (37.0 ± 0.1 °C, 5.0 ± 0.1% CO_2, 99.5 ± 0.1% RH). Post-rendering of the obtained images of optical sections was performed using Olympus cellSence software (Olympus licensed).

Assay of cell viability, ROS, cell death types and caspases. Cell viability was determined using the NIR dye ($\lambda_{Ex}/\lambda_{Em}$ = 633/720 nm) as parts of "LIVE/DEAD Near IR Viability Kit" (Thermo Scientific, L34994). The concentration of free oxygen species in living cells was determined fluorimetrically using the "Cellular Reactive Oxygen Species Detection Assay Kit – Orange Fluorescence" (Abcam, ab186028). The cell death types and content of active caspases was determined using the "Apoptosis/Necrosis Assay Kit (Abcam ab176749)", "Autophagy Assay Kit" (Ab-

cam, ab139484) and "Caspase-3, Caspase-8 and Caspase-9 Multiplex Activity Assay Kit" (Abcam ab219915) respectively. The caspases multiplex activity assay kit uses DEVD-ProRed™, IETD-R110 and LEHD-AMC as fluorogenic indicators for caspase 3, caspase 8 and caspase 9 activity respectively. Upon caspase cleavage, three distinct fluorophores are released: ProRed™ (red fluorescence), R110 (green fluorescence) and AMC (blue fluorescence), which can be readily monitored in a single assay due to their nice spectral separation. Cells were observed using the same parameters of lasers and photomultipliers.

Statistical analysis. The data were statistically analyzed using the ANOVA dispersion analysis using Statistica 7.0 software (StatSoft Inc., USA). We calculated standard mean values (x) and standard deviation (SD). Differences between groups were determined using the Tukey test, where the differences were considered reliable at $P < 0.05$ (taking into account Bonferroni correction).

Results

Figure 1 shows the three-dimensional distribution of fibroblasts and keratinocytes in the transplant 20 minutes after the injection of a cell mixture into a porous scaffold without and after irradiation. In both groups, the transplant exhibited a similar shape, volume, and cell distribution within the volume (Table 1).

Figure 2 shows the localization of the skin equivalent cells prior to transplantation (blue marker), as well as the individual migration tracks of fibroblasts and keratinocytes (green and red markers, respectively) on the 2nd, 4th, and 6th day after the injection of the cell mixture into a three-dimensional culture. The quantitative analysis of the tracks is provided in Table 2.

It is evident that as early as the 2nd day of observation, an area with an increased density of cells of skin equivalent is formed around the transplant. This may be the result of cell migration from the volume of the equivalent to the periphery of the transplant, and the transplant with a higher content of nutrients is a chemoattractant for the cells of the equivalent. At the same time, in the non-irradiated skin equivalent, the cell density at the periphery of the transplant is significantly higher due to their greater viability and, consequently, mobility, compared to the cells in the irradiated dermal equivalent.

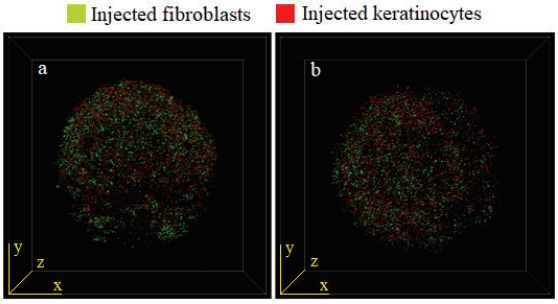

Fig. 1. Confocal laser scanning microscopy (CLSM) 3D visualization (fluorescence z-stack mode) of injected fibroblasts and keratinocytes into irradiated (*a*) and non-irradiated (*b*) porous alginate scaffold: 60/1.2 NA water-immersion objective

Table 1
The morphometric parameters of cellular transplantants into irradiated and non-irradiated porous alginate scaffold (x ± SD, n = 24, 20 minutes after the injection)

Morphometric parameters	Convex hull perimeter	Aspect ratio (D_{max}/D_{min})	Volume, $\mu m^2 \times 10^3$
Non-irradiated scaffold	0.71 ± 0.10	1.38 ± 0.12	411.3 ± 34.2
Irradiated scaffold	0.74 ± 0.11	1.35 ± 0.08	462.4 ± 27.5

Notes: the convex hull perimeter and aspect ratio of ideal sphere is 1.0; no statistical differences in each column were found.

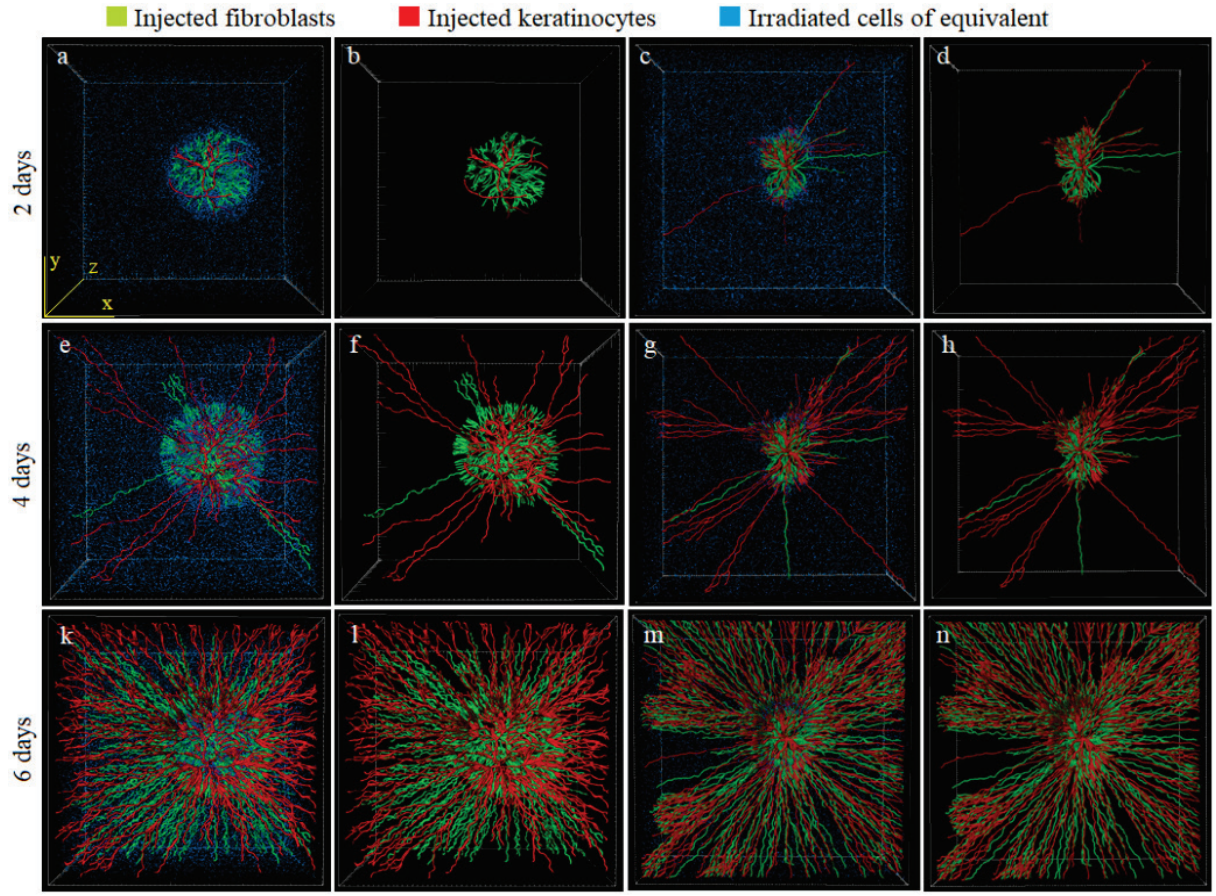

Fig. 2. Confocal laser scanning microscopy (CLSM) 3D tracking visualization (fluorescence z-stack mode) of irradiated fibroblasts and keratinocytes (blue tracking dye) and injected fibroblasts (green tracking dye) and injected keratinocytes (red tracking dye) into irradiated (*c–d, g–h, m–n*) and non-irradiated (*a–b, e–f, k–l*) scaffold on the 2, 4 and 6 days: 60/1.2 NA water-immersion objective

Table 2
Migration speed (v, μm/h) and net displacement (Dnet, μm) injected fibroblasts and keratinocytes into irradiated porous alginate scaffold (x ± SD, n = 24)

Days	Experimental groups	Fibroblasts		Keratinocytes	
		v	Dnet	v	Dnet
2	Non-irradiated scaffold	30.2 ± 2.1^{a}	170.6 ± 9.4^{a}	32.3 ± 1.1^{a}	194.1 ± 5.3^{a}
	Irradiated scaffold	28.5 ± 1.8^{a}	256.5 ± 7.3^{b}	36.1 ± 1.8^{b}	243.5 ± 10.5^{b}
4	Non-irradiated scaffold	32.7 ± 1.6^{a}	181.2 ± 7.5^{a}	37.2 ± 3.2^{b}	208.3 ± 6.4^{c}
	Irradiated scaffold	31.9 ± 1.5^{a}	428.5 ± 4.8^{c}	55.9 ± 2.5^{c}	537.7 ± 11.8^{d}
6	Non-irradiated scaffold	34.6 ± 3.0^{a}	318.1 ± 12.1^{d}	41.7 ± 1.7^{b}	275.0 ± 9.5^{e}
	Irradiated scaffold	46.2 ± 2.4^{b}	765.7 ± 14.5^{e}	68.3 ± 2.4^{d}	791.4 ± 10.7^{f}

Notes: means in each column followed by different letters are significantly different from one another on the results of comparison using the Tukey test ($P < 0.05$) with Bonferroni correction.

Throughout all days of observation, cell migration of both fibroblasts and keratinocytes within the transplant occurs. However, the nature of transplant cell migration in non-irradiated and irradiated skin equivalent was different.

Thus, on the 2nd day of observation in both groups, the nature of cell migration predominantly exhibited a local character. There was no difference in average speed of cell migration, persistence of direction (net displacement), and overall direction between fibroblasts and keratinocytes injected into the non-irradiated three-dimensional culture. However, in the irradiated culture, both fibroblasts and keratinocytes showed significant heterogeneity in all of these parameters. A distinct group of cells (7.8% of the total injected number of cells) exhibited higher migration speed and persistence of direction. At the same time, 98.2% of migrating keratinocytes and 4.1% of migrating fibroblasts shared the same overall direction, moving toward the upper surface of the skin equivalent.

On the 4th day of observation, the heterogeneity of the transplant cells according to migration parameters was also manifested in the non-irradiated skin equivalent. At the same time, 93.7% of cell migration within the transplant exhibited a local character, and the proportion of keratinocytes with higher migration speed and persistence of direction towards the upper surface of the skin equivalent was 27.6%.

By the 6th day of observation, clear and distinct differences in the migration nature of fibroblasts and keratinocytes following the injection of the cell mixture into the skin equivalent, with or without irradiation, were observed. Thus, 73.8% of migrating fibroblasts of the transplant moved exclusively within the lower 2/3 of the three-dimensional culture, with 61.3% of them maintaining a local migration pattern toward the periphery of the transplant.

Only 1.9% of fibroblasts retained a persistent movement towards the upper surface of the non-irradiated skin equivalent. At the same time, 27.5% of migrating keratinocytes exhibited local migration at the periphery of the transplant, while 72.1% had a different overall direction compared to fibroblasts; they migrated exclusively towards the upper surface of the non-irradiated equivalent skin.

The pattern of cell migration in the irradiated three-dimensional culture on the 6th day of observation differed from the pattern of cell migration in the non-irradiated culture. Specifically, 75.8% of migrating fibroblasts and 98.2% of migrating keratinocytes within the transplant moved towards the upper surface or migrated within the upper plane of the irradiated equivalent. On the other hand, 23.7% of migrating fibroblasts and 2.4% of migrating keratinocytes within the transplant exhibited a local migration pattern at the periphery of the transplant, possibly due to low viability.

At the same time, it was shown that over the entire observation period, the total number of cells in the skin equivalent remained unchanged, since the skin equivalent at the beginning of the experiment was a stable three-dimensional culture, and the cells were in a state of contact inhibition and did not proliferate. However, the number of cells in the irradiated culture significantly decreased each day of observation, and by the 6th day, it had reduced by 46.1%. Nevertheless, it was found that the reduction in the number of cells occurred unevenly, with an area where the number of skin equivalent cells decreased by only 11.8% – this was at the periphery of the transplant. It is possible that the introduced fibroblasts, which have a local nature of migration at the periphery of the transplant, "support" the viability of cells in their microenvironment. Such an autocrine effect can be provided by the secretion of a number of growth factors, in particular the connective tissue growth factor (CTGF), the synthesis of which by the fibroblasts of the transplant stimulates the synthesis of the transforming growth factor TGF-beta. TGF-beta activates the chemotaxis of microenvironment fibroblasts and sustains the metabolism of exhausted or damaged cells incapable of autoregulation.

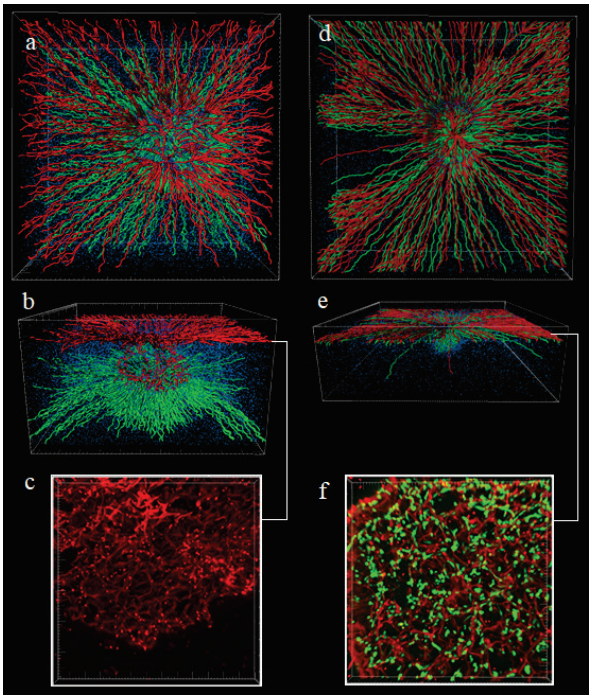

Fig. 3. Confocal laser scanning microscopy (CLSM) 3D tracking (*a*, *b*, *d*, *e*) and single optical section (*c*, *f*) visualization of irradiated fibroblasts and keratinocytes (blue tracking dye) and injected fibroblasts (green tracking dye) and injected keratinocytes (red tracking dye) on surface of irradiated (*d*, *e*, *f*) and non-irradiated (*a*, *b*, *c*) scaffold on 6 days. 60/1.2 NA water-immersion objective

It was shown that due to the different migration patterns of fibroblasts and keratinocytes in the non-irradiated and irradiated culture, there were significant differences in the specific cellular composition of the upper, keratinocyte-enriched layer of the dermal equivalent on the 6th day (Fig. 3). Thus, in the non-irradiated culture on the 6th day of observation, a keratinocyte-enriched layer was formed, in which the content of fibroblasts migrating from the transplant was less than 0.9%. However, in the irradiated culture on the same day of observation, in the upper keratinocyte-enriched layer, the proportion of fibroblasts was 37.2% of the total number of cells.

Cells of the equivalent in culture die as a result of either direct effects of ionizing radiation, or due to hyperproduction of reactive oxygen species (ROS) by both the cells (Fig. 4, 5) and their microenvironment, as a consequence of the well-known radiolysis effects of polymers, in particular alginate, which comprises the framework of the dermal equivalent.

The transplantation of cells into the irradiated culture did not lead to significant changes in the concentration of ROS on the 2nd, 4th and 6th day after irradiation of the equivalent. However, by the 6th day, the concentration of reactive oxygen species was nearly 1.6 times (35.2%) lower compared to the irradiated equivalent without transplantation and decreased by 35.2% (Fig. 5).

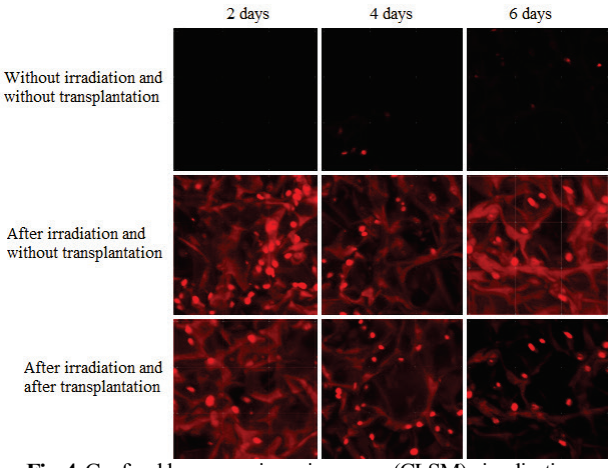

Fig. 4. Confocal laser scanning microscopy (CLSM) visualization of ROS-specific fluorescence in fibroblasts and keratinocytes of irradiated and non-irradiated scaffold. 60/1.2 NA water-immersion objective

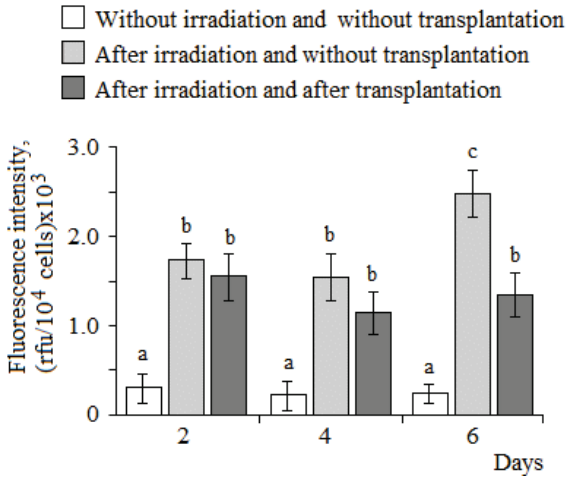

Fig. 5. The content of reactive oxygen species in fibroblasts and keratinocytes of irradiated and non-irradiated scaffold (x ± SD, n = 24): different letters indicate samplings that significantly differ one from another according to the Tukey test with the Bonferroni correction

In addition to the uneven distribution of the number of cells within the irradiated equivalent volume against the background of a decrease in their number it is demonstrated that the cells within the irradiated equivalent are unevenly distributed in the volume according to their viability (Fig. 6).

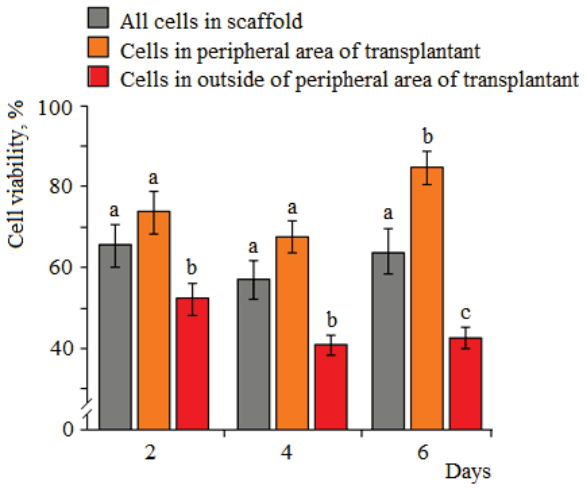

Fig. 6. Viability of the fibroblasts and keratinocytes in irradiated alginate porous scaffold (x ± SD, n = 24): different letters indicate significant differences between the groups in each day according to the Tukey test with the Bonferroni correction

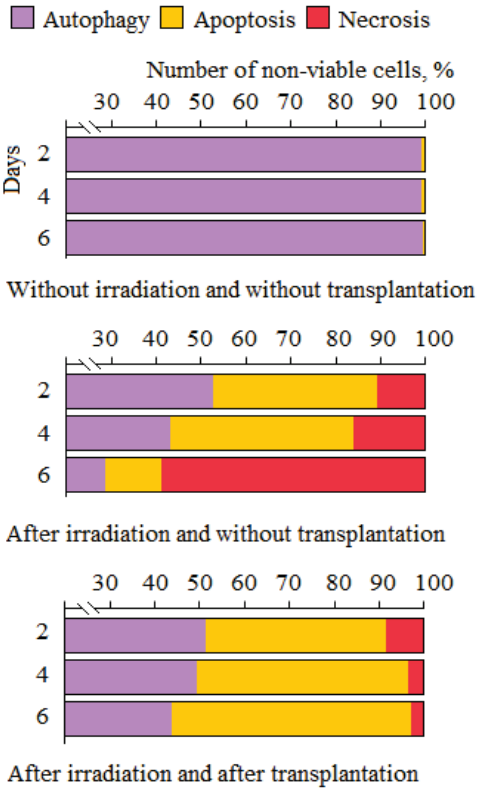

Fig. 7. Death types of the fibroblasts and keratinocytes in alginate porous scaffold

Table 3
The content of caspases 3, 8 and 9 in fibroblasts and keratinocytes in alginate porous scaffold (rfu/10^3 cells)

Days	Experimental groups	Caspase 3	Caspase 8	Caspase 9
2	Without irradiation Without transplantation	12.7 ± 2.4^{a}	14.5 ± 2.1^{a}	3.1 ± 1.5^{a}
	After irradiation Without transplantation	87.3 ± 5.1^{b}	33.9 ± 4.6^{b}	104.5 ± 4.5^{b}
	After irradiation After transplantation	61.5 ± 3.6^{c}	71.5 ± 2.9^{c}	88.2 ± 3.1^{c}
4	Without irradiation Without transplantation	10.5 ± 2.1^{a}	12.3 ± 1.8^{a}	2.4 ± 1.1^{a}
	After irradiation Without transplantation	115.7 ± 8.4^{d}	37.5 ± 2.9^{b}	144.8 ± 11.2^{f}
	After irradiation After transplantation	94.7 ± 3.3^{b}	93.8 ± 3.6^{d}	101.4 ± 2.8^{b}
6	Without irradiation Without transplantation	14.1 ± 2.5^{a}	14.7 ± 3.3^{a}	6.1 ± 2.8^{d}
	After irradiation Without transplantation	31.7 ± 3.9^{e}	8.6 ± 2.8^{e}	39.4 ± 2.2^{e}
	After irradiation After transplantation	155.3 ± 11.4^{f}	164.5 ± 4.1^{f}	115.7 ± 5.1^{b}

Notes: means in each column followed by different letters are significantly different from one another on the results of comparison using the Tukey test ($P < 0.05$) with Bonferroni correction.

It has been found that cells in the non-irradiated dermal equivalent primarily underwent autophagy-induced cell death (Fig. 7). Thus, the average percentage (2–6 days of observation) of non-viable cells in non-irradiated culture is 10.9%. Among these, the majority (99.2%) underwent cell death via autophagy, while only 0.8% underwent apoptosis. Cell death by necrosis was not observed.

It has been demonstrated that cell death through autophagy predominantly occurs in non-proliferating cells (G0 phase or terminal differentiation), which aligns with the conditions in a stable three-dimensional culture where cells, due to contact inhibition, hardly divide or migrate.

After irradiation, there was a significant increase in the proportion of cells undergoing apoptosis. On the 2–4th day of observation, cells primarily underwent apoptosis, necrotic cells accounted for a smaller percentage.

However, the percentage of apoptotic and necrotic cells increased with the duration of observation. On the 6th day, the cells of the irradiated culture without transplantation primarily underwent necrosis, indicating the depletion of cellular energy resources needed to sustain the energy-demanding apoptotic pathway.

In support of this assumption, the results of determining the profile of active caspases in the irradiated equivalent should be mentioned (Table 3).

Thus, on the 2–4th day of observation, the irradiated culture experienced an increase in the content of active caspase 3 (the main effector caspase that initiates proteolytic processes within cells) and a significant increase in the content of active caspase 9, while the content of active caspase 8 remained unchanged. This indicates that cells in the irradiated culture underwent apoptosis through the mitochondrial pathway, rather than the receptor-mediated pathway. This is consistent with the data obtained regarding the hyperproduction of reactive oxygen species by cells after irradiation.

Mitochondria are able to directly induce cell death by increasing the permeability of the mitochondrial outer membrane, which leads to the release of cytochrome *c* into the cytosol. Cytochrome *c*, in turn, plays a role in forming the apoptosome, which interacts with effector procaspase 9, activating it. On the 6th day of observation, the content of active caspases 3, 8, 9 significantly decreased due to a sharp reduction in the proportion of cells undergoing apoptosis and the activation of necrotic processes incompatible with transcription/translation processes.

A number of authors have shown that the predominance of caspase 9 content in irradiated tissues and serum of patients after radiation therapy is accompanied by low efficacy of accompanying pharmacological support therapy. Transplantation of a mixture of fibroblasts and keratinocytes into the irradiated equivalent led to a significant increase in the content of active effector caspases 3, 8, and 9 from the 2nd to the 6th day of observation. However, compared to the irradiated culture without transplantation, the significant differences in the content of different types of caspases under transplantation conditions were shown. In the irradiated culture, caspase 9 was activated while the content of caspase 8 remained unchanged. However, in the presence of the transplant, both types of caspases were activated. Starting from the 6th day, the content of active caspase 8 became significantly higher than the content of caspase 9.

Discussion

As was shown, active proliferation of fibroblasts and keratinocytes of the transplant began on the 6th day, and by that time, they were distributed throughout the irradiated volume of the dermal equivalent. It is probable that proliferating and actively synthesizing cells of the transplant significantly reduce the concentration of reactive oxygen species through the synthesis of antioxidant defense enzymes (Jena et al., 2023; Chettouh-Hammas et al., 2023). In a series of studies, it has been demonstrated that culturing keratinocytes under unfavorable conditions without the support of fibroblasts or mesenchymal cells leads to the complete death of keratinocytes through apoptosis after 14 days of cultivation (Tanaka et al., 2022, Xu et al., 2023). However, when keratinocytes are cultured on a collagen gel with fibroblasts, they do not undergo apoptosis and actively proliferate (Tahri et al., 2023; Zhang et al., 2023). This result can be explained by the fact that fibroblasts synthesize keratinocyte growth factor (KGF), epidermal growth factor (EGF), colony-stimulating growth factor/interleukin (IL6), fibroblast growth factor (FGF10), which stimulate keratinocytes to synthesize interleukin IL1, which stimulates fibroblasts to the synthesis of KGF (Yen et al., 2014; Bártolo et al., 2022). Such a system of mutually regulating positive feedback leads, firstly, to the migration of fibroblasts after keratinocytes along the interleukin IL1 gradient, and secondly, provides mutual "support" of the transplant cells in the conditions of a relatively aggressive cytotoxic environment of the post-irradiated culture. At the same time, it was shown on models of mechanical skin damage that one of the early reparative regulatory molecular mechanisms is the synthesis of the keratinocyte growth factor KGF7, which binds to the FGFR2IIIb receptor on keratinocytes and stimulates them to synthesize the transforming growth factor of fibroblasts TGFβ1. This leads to the differentiation of fibroblasts into myofibroblasts. Compared to fibroblasts, myofibroblasts are characterized by an inability to migrate, hyperproduction of total protein (in particular, collagen type 1), TGFβ1, TGFβ2. These transforming growth factors stimulate keratinocytes in the microenvironment to regenerate, which leads to sclerosing of the damaged tissue and the formation of scars (Lee, 2022; Pot et al., 2023). It is possible that a similar mechanism should also be triggered under conditions of irradiation.

It was shown that cells in the non-irradiated dermal equivalent primarily undergo autophagy-induced cell death while cell death by necrosis was not observed. In principle, this corresponds with existing literature data, indicating that autophagy is the pathway through which a normal, untransformed cell culture "clears out" cells that have exhausted their limit of division numbers or have critical disruptions in the mechanisms of division and transcription/translation (Yang et al., 2023).

Starting from the 6th day, the content of active caspase 8 became significantly higher than the content of caspase 9. This indicates that in cells of the irradiated culture under transplantation conditions, the receptor-mediated apoptosis pathway dominates through the plasma membrane receptor Fas, which interacts with the FADD domain of the Fas receptor, thereby activating caspase 8 (Dixit, 2023). A series of studies have demonstrated that the molecular mechanisms of the receptor-mediated apoptosis pathway have cross-links with the molecular mechanisms of autophagy. For example, the Fas-FADD-caspase 8 apoptosome can activate the ubiquitin-like Atg5-Atg12 complex, which participates in autophagosome membrane elongation. Thus, the change in the path of cell apoptosis during transplantation makes the process of cell death through the receptor-mediated mechanism significantly more controlled (Pang & Vince, 2023).

It has been shown that along with the change in the apoptosis induction mechanism during cell transplantation into the irradiated equivalent, there is a significant reduction in the number of necrotic cells, starting from the 4th day. A number of authors have shown on various experimental models that programmed necrosis can be inhibited by the action of antioxidants on cells (Miklós & Horváth, 2023; Sun et al., 2023). It is probable that proliferating and actively synthesizing cells in the transplant significantly reduce the levels of free oxygen radicals through the synthesis of antioxidant defense enzymes on the 6th day. Alternatively, an increase in the content of active caspases may play a role in suppressing the activity of RIP protein kinase, an initiator of necrosis in cells (Moriwaki & Chan, 2014; Urwyler-Rösselet et al., 2023).

Conclusion

The cells of the non-irradiated dermal equivalent mainly die through autophagy, while in the irradiated equivalent, necrosis is the primary mode of cell death. However, after transplantation, apoptosis becomes the dominant mode of cell death. In the irradiated culture, cells die primarily through the mitochondrial apoptosis pathway (as indicated by a higher content of active caspase 9), whereas in the irradiated culture with transplantation, the receptor-mediated apoptosis pathway predominates (as indicated by a higher content of active caspase 8). The obtained results can be important for radiobiology and radiomedicine, because in addition to advancing fundamental knowledge, they can be used for the development of new effective methods of therapy for radiation burns, chronic ulcers and wounds of various etiologies.

The authors express their gratitude to L.Y. Vasyliev, Physician-in-Chief of the State Organization "Grigoriev Institute for Medical Radiology and Oncology of the National Academy of Medical Sciences of Ukraine", and Radiologist A. V. Trofimov for consultations and technical operator work during the irradiation on the basis of the Institute.

The research was supported by research project 0123U103180 of V. N. Karazin Kharkiv National University and the Fund for Development and Modernization of Educational and Scientific Equipment of V. N. Karazin Kharkiv National University (order No. 0304-1/439), Kharkiv, Ukraine.

The authors declare no conflict of interests.

References

Arnold, K. M., Flynn, N. J., Raben, A., Romak, L. Y. Y., Dicker, A. P., Mourtada, F., & Sims-Mourtada, J. (2018). The impact of radiation on the tumor microenvironment: Effect of dose and fractionation schedules. Cancer Growth Metastasis, 11, 1179064418761639.

Bártolo, I., Reis, R. L., Marques, A. P., & Cerqueira, M. T. (2021). Keratinocyte growth factor-based strategies for wound re-epithelialization. Tissue Engineering, Part B: Reviews, 28(3), 665–676.
Brahme, A. (2023). TP53 and the ultimate biological optimization steps of curative radiation oncology. Cancers, 15(17), 4286.
Capuzzimati, M., Hough, O., & Liu, M. (2022). Cell death and ischemia-reperfusion injury in lung transplantation. The Journal of Heart and Lung Transplantation, 41(8), 1003–1013.
Chettouh-Hammas, N., Fasani, F., Boileau, A., Gosset, D., Busco, G., & Grillon, C. (2023). Improvement of antioxidant defences in keratinocytes grown in physioxia: Comparison of 2D and 3D models. Oxidative Medicine and Cellular Longevity, 2023, 6829931.
Dixit, V. M. (2023). The road to death: Caspases, cleavage, and pores. Science Advances, 9(17), eadi2011.
Galluzzi, L., & Myint, M. (2023). Cell death and senescence. Journal of Translational Medicine, 21(1), 425.
Hofmann, E., Fink, J., Pignet, A. L., Schwarz, A., Schellnegger, M., Nischwitz, S. P., Holzer-Geissler, J. C. J., Kamolz, L. P., & Kotzbeck, P. (2023). Human *in vitro* skin models for wound healing and wound healing disorders. Biomedicines, 11(4), 1056.
Hu, X. M., Li, Z. X., Lin, R. H., Shan, J. Q., Yu, Q. W., Wang, R. X., Liao, L. S., Yan, W. T., Wang, Z., Shang, L., Huang, Y., Zhang, Q., & Xiong, K. (2021). Guidelines for regulated cell death assays: A systematic summary, a categorical comparison. Frontiers in Cell and Developmental Biology, 9, 634690.
Jena, A. B., Samal, R. R., Bhol, N. K., & Duttaroy, A. K. (2023). Cellular Red-Ox system in health and disease: The latest update. Biomedicine and Pharmacotherapy, 162, 114606.
Jiao, Y., Cao, F., & Liu, H. (2022). Radiation-induced cell death and its mechanisms. Health Physics, 123(5), 376–386.
Kot, Y. G., Altukhova, L. V., Kot, K. V., Morozova, K. S., & Persky, Y. E. (2015). Biochemical mechanisms of skin radiation burns inhibition and healing by the volumetric autotransplantation of fibroblasts and keratinocytes with fibroblasts composition. Regulatory Mechanisms in Biosystems, 6(2), 125–132.
Lee, S. Y. (2022). Endothelial cell derived connective tissue growth factor stimulates fibroblast differentiation into myofibroblasts through integrin αVβ3. Experimental and Therapeutic Medicine, 25(1), 30.
Lomonaco, S. L., Finniss, S., Xiang, C., Decarvalho, A., Umansky, F., Kalkanis, S. N., Mikkelsen, T., & Brodie, C. (2009). The induction of autophagy by gamma-radiation contributes to the radioresistance of glioma stem cells. The International Journal of Cancer, 125(3), 717–722.
Lu, G., Wang, Y., Shi, Y., Zhang, Z., Huang, C., He, W., Wang, C., & Shen, H. M. (2022). Autophagy in health and disease: From molecular mechanisms to therapeutic target. MedComm, 3(3), e150.
Machado, I. F., Palmeira, C. M., & Rolo, A. P. (2023). Preservation of mitochondrial health in liver ischemia/reperfusion injury. Biomedicines, 11(3), 948.
Miklós, Z., & Horváth, I. (2023). The role of oxidative stress and antioxidants in cardiovascular comorbidities in COPD. Antioxidants, 12(6), 1196.
Monjazeb, A. M., Schalper, K. A., Villarroel-Espindola, F., Nguyen, A., Shiao, S. L., & Young, K. (2020). Effects of radiation on the tumor microenvironment. Seminars in Radiation Oncology, 30(2), 145–157.
Moriwaki, K., & Chan, F. K. (2014). Necrosis-dependent and independent signaling of the RIP kinases in inflammation. Cytokine and Growth Factor Reviews, 25(2), 167–74.
Mott, J. H. L., & West, N. S. (2021). Essentials of depth dose calculations for clinical oncologists. Clinical Radiology, 33(1), 5–11.
Obata, H., Ogawa, M., & Zalutsky, M. R. (2023). DNA repair inhibitors: Potential targets and partners for targeted radionuclide therapy. Pharmaceutics, 15(7), 1926.
Owusu, S. B., Hudik, E., Férard., C., Dupré-Crochet, S., Addison, E. C. D. K., Preko, K., Bizouarn, T., Houée-Levin, C., & Baciou, L. (2021). Radiation-induced reactive oxygen species partially assemble neutrophil NADPH oxidase. Free Radical Biology and Medicine, 164, 76–84.
Pang, J., & Vince, J. E. (2023). The role of caspase-8 in inflammatory signalling and pyroptotic cell death. Seminars in Immunology, 70, 101832.
Park, W., Wei, S., & Kim, B. S. (2023). Diversity and complexity of cell death: A historical review. Experimental and Molecular Medicine, 55, 1573–1594.
Pot, S. A., Lin, Z., Shiu, J., Benn, M. C., & Vogel, V. (2023). Growth factors and mechano-regulated reciprocal crosstalk with extracellular matrix tune the keratocyte-fibroblast/myofibroblast transition. Scientific Reports, 13(1), 11350.
Rasouli, M., Fattahi, R., Nuoroozi, G., Zarei-Behjani, Z., Yaghoobi, M., Hajmohammadi, Z., & Hosseinzadeh, S. (2023). The role of oxygen tension in cell fate and regenerative medicine: Implications of hypoxia/hyperoxia and free radicals. Cell Tissue Bank, 2023, 37365484.
Roy, A., Bera, S., Saso, L., & Dwarakanath, B. S. (2022). Role of autophagy in tumor response to radiation: Implications for improving radiotherapy. Frontiers in oncology, 12, 957373.
Saleh, T., As Sobeai, H., Alhoshani, A., Alhazzani, K., Almutairi, M., & Alotaibi, M. (2022). Effect of autophagy inhibitors on radiosensitivity in dna repair-proficient and -deficient glioma cells. Medicina, 58, 889.
Shen, S., Shao, Y., & Li, C. (2023). Different types of cell death and their shift in shaping disease. Cell Death Discovery, 9, 284.
Sia, J., Szmyd, R., Hau, E., & Gee, H. E. (2020). Molecular mechanisms of radiation-induced cancer cell death: A primer. Frontiers in Cell and Developmental Biology, 8, 41.
Sun, Q., Ma, H., Zhang, J., You, B., Gong, X., Zhou, X., Chen, J., Zhang, G., Huang, J., Huang, Q., Yang, Y., Ai, K., & Bai, Y. (2022). A self-sustaining antioxidant strategy for effective treatment of myocardial infarction. Advanced Science, 10(5), e2204999.
Tahri, S., Maarof, M., Masri, S., Che Man, R., Masmoudi, H., & Fauzi, M. B. (2023). Human epidermal keratinocytes and human dermal fibroblasts interactions seeded on gelatin hydrogel for future application in skin *in vitro* 3-dimensional model. Frontiers in Bioengineering and Biotechnology, 11, 1200618.
Takács-Vellai, K. (2023). Apoptosis and autophagy, different modes of cell death: How to utilize them to fight diseases? International Journal of Molecular Sciences, 24(14), 11609.
Tanaka, K., Ogino, R., Yamakawa, S., Suda, S., & Hayashida, K. (2022). Role and function of mesenchymal stem cells on fibroblast in cutaneous wound healing. Biomedicines, 10(6), 1391.
Urwyler-Rösselet, C., Tanghe, G., Devos, M., Hulpiau, P., Saeys, Y., & Declercq, W. (2023). Functions of the RIP kinase family members in the skin. Cellular and Molecular Life Sciences, 80(10), 285.
Van Erp, A. C., Hoeksma, D., Rebolledo, R. A., Ottens, P. J., Jochmans, I., Monbaliu, D., Pirenne, J., Leuvenink, H. G. D., & Decuypere, J. P. (2017). The crosstalk between ROS and autophagy in the field of transplantation medicine. Oxidative Medicine and Cellular Longevity, 2017, 7120962.
Villalpando-Rodriguez, G. E., & Gibson, S. B. (2021). Reactive oxygen species (ROS) regulates different types of cell death by acting as a rheostat. Oxidative Medicine and Cellular Longevity, 2021, 9912436.
Wong, J. H. D., Zaili, Z., Abdul Malik, R., Bustam, A. Z., Saad, M., Jamaris, S., Mosiun, J. A., Mohd Taib, N. A., Ung, N. M., & See, M. H. (2021). Evaluation of skin dose and skin toxicity in patients undergoing intraoperative radiotherapy for early breast cancer. The Journal of Applied Clinical Medical Physics, 22(8), 139–147.
Wu, H. W., Chen, H. D., Chen, Y. H., Mao, X. L., Feng, Y. Y., Li, S. W., & Zhou, X. B. (2023). The effects of programmed cell death of mesenchymal stem cells on the development of liver fibrosis. Stem Cells International, 2023, 4586398.
Xu, R., Wu, M., Wang, Y., Li, C., Zeng, L., Wang, Y., Xiao, M., Chen, X., Geng, S., Lai, P., Du, X., & Weng, J. (2023). Mesenchymal stem cells reversibly dedifferentiate myofibroblasts to fibroblast-like cells by inhibiting the TGF-β-SMAD2/3 pathway. Molecular Medicine, 29(1), 59.
Yang, J., Kim, W., & Kim, D. R. (2023). Autophagy in cell survival and death. International Journal of Molecular Sciences, 24(5), 4744.
Yen, T. T., Thao, D. T., & Thuoc, T. L. (2014). An overview on keratinocyte growth factor: From the molecular properties to clinical applications. Protein & Peptide Letters, 21(3), 306–317.
Yoo, J. G., Lee, Y. K., & Lee, K. H. (2023). Enhancing autophagy leads to increased cell death in radiation-treated cervical cancer cells. The Journal of Obstetrics and Gynaecology, 43(1), 2171281.
Zein, L., Fulda, S., Kögel, D., & van Wijk, S. J. L. (2020). Organelle-specific mechanisms of drug-induced autophagy-dependent cell death. Matrix Biology, 100–101, 54–64.
Zhang, G., Wang, J., Zhao, Z., Xin, T., Fan, X., Shen, Q., Raheem, A., Lee, C., R., Jiang, H., & Ding, J. (2022). Regulated necrosis, a proinflammatory cell death, potentially counteracts pathogenic infections. Cell Death and Disease, 13, 637.
Zhang, Y., Wang, Y., Li, Y., Yang, Y., Jin, M., Lin, X., Zhuang, Z., Guo, K., Zhang, T., & Tan, W. (2023). Application of collagen-based hydrogel in skin wound healing. Gels, 9, 185.
Zhao, Y., Main, K., Aujla, T., Keshavjee, S., & Liu, M. (2023). Necroptosis in organ transplantation: Mechanisms and potential therapeutic targets. Cells, 12(18), 2296.